

The distribution and kinematics of interstellar O VI in the Milky Way

R. Sarma^{1*}, A. Pathak^{2†}, Jayant Murthy³ and J. K. Sarma²

¹*Department of Physics, Hojai College, Hojai, 782435, India*

²*Department of Physics, Tezpur University, 784028, India*

³*Indian Institute of Astrophysics, Koramangala, Bangalore 560 034, India*

ABSTRACT

We present the results of a survey of interstellar O VI absorption in the Milky Way (MW) towards 69 stars in the Large Magellanic Cloud (LMC) obtained with the *Far Ultraviolet Spectroscopic Explorer (FUSE)*. The integrated MW O VI column densities $\log N(\text{O VI})$ are in the range from 13.68 to 14.73 with a mean of $14.26^{+0.07}_{-0.09}$ atoms cm^{-2} . The O VI exponential scale height is found to be 2.28 ± 1.06 kpc. The O VI column density correlates with the Doppler parameter b . The O VI velocity dispersion ranges from 14.0 to 91.6 with an average value of 62.7 km s^{-1} . These high values of velocity dispersion reveal the effect of turbulence, multiple velocity components and collision on broad O VI profiles. There is a significant variation of O VI column density on all scales studied ($0.0025^\circ - 6.35^\circ$). The smallest scale for which O VI column density variations has been found is $\Delta\theta \sim 9''$. Comparison of the O VI velocity profiles with Fe II indicates the presence of intermediate velocity cloud (IVC) and/or high velocity cloud (HVC) components in the O VI absorption.

Key words: ISM:atoms–ISM:galaxies:Milky Way

1 INTRODUCTION

Highly ionized gas spanning the temperature range from 10^5 to 10^7 K is an important constituent of the interstellar medium (ISM) of galaxies. Species in the hot phase of the ISM (Si IV, C IV, N V, O VI, etc.) show strong transitions in the ultraviolet (UV). Important lines amongst these are the O^{+5} (O VI) absorptions at 1032 Å and 1038 Å. O VI is unlikely to arise from photoionization as 113.9 eV is required to remove one more electron from O V but is rather produced in the ISM through collisional ionization at temperatures of about 3×10^5 K (Indebetouw & Shull 2004; Cox 2005). Such temperatures represent the interface between the warm ($T \sim 10^4$ K) and the hot ($T > 10^6$ K) phases of the interstellar gas and a detailed analysis of the O VI absorption aids in understanding the total abundance and the processes leading to its formation in the ISM (Wakker et al. 2012).

The first observations of O VI absorption were made with the *Copernicus* satellite (Jenkins 1978a,b) followed by observations made with the *Hopkins Ultraviolet Telescope (HUT)* (Dixon et al. 1996). The *Far Ultraviolet Spectroscopic Explorer (FUSE)* (Moos et al. 2000; Sahnou et al. 2000) launched in 1999 June contributed significantly to the observation of O VI absorption with much higher resolution

and signal to noise. *FUSE* had a far-ultraviolet (FUV) wavelength coverage between 905 – 1187 Å with a resolution of $\sim 15,000 - 20,000$ near the O VI line absorption wavelengths. The study of O VI absorption in the ISM of galaxies with *FUSE* has given us information about the formation and distribution of O VI in the MW and the Magellanic Clouds that adds to our knowledge of varying ISM conditions in environments of different metallicities (Howk et al. (2002a); Savage et al. (2000); Wakker et al. (2003); Oegerle et al. (2005); Savage & Lehner (2006); Welsh & Lallement (2008); Pathak et al. (2011)). Apart from absorption studies, *FUSE* has also been used to observe the O VI spectra in emission from the diffuse ISM in the MW (Shelton et al. 2001; Dixon et al. 2006; Dixon & Sankrit 2008), from superbubbles (SBs) and in the LMC (Sankrit & Dixon 2007). O VI absorption studies at low redshifts trace the warm-hot intergalactic medium (WHIM) and are important contributor to models of the cosmological problem of missing baryons (Tepper-Garcia et al. 2011).

2 O VI IN THE MILKY WAY

Although the first observations of hot interstellar gas of the MW were made with the *Copernicus* satellite (York 1974; Jenkins 1978a), it was not until the launch of the *FUSE* satellite that large scale observations of O VI absorption

* e-mail: sharma.rathin@gmail.com

† e-mail: amitpah@gmail.com

in the MW began. Strong O VI absorption was detected along 10 out of 11 lines of sight by Savage et al. (2000) with $\log N(\text{O VI})$ ranging from 13.80 to 14.64 atoms cm^{-2} while Howk et al. (2002b) found a mean column density of $14.52_{-0.14}^{+0.10}$ atoms cm^{-2} in the direction of the LMC. Savage et al. (2005) report *FUSE* observations of O VI absorption towards 100 extragalactic lines of sight finding that the average $\log N(\text{O VI})$ is 14.36 atoms cm^{-2} . Bowen et al. (2008) studied absorption lines of O VI towards 148 early-type stars situated at distances ≥ 1 kpc and found an average O VI midplane density of $1.3 \times 10^{-8} \text{ cm}^{-3}$.

Pathak et al. (2011) surveyed the O VI absorption in the LMC towards 70 lines of sight using *FUSE* and noted the presence of a MW component in each of these lines of sight. We have analysed all these sightlines and report our findings here.

3 OBSERVATIONS AND DATA REDUCTION

A detailed description of the *FUSE* mission and instruments has been given by Moos et al. (2000) and Sahnou et al. (2000). *FUSE* consists of two channels (SiC and LiF) optimized for short and long wavelength observations. These channels are further divided into eight segments; the SiC 1A, SiC 2A, SiC 1B, SiC 2B covering the wavelength range 905 - 1105 Å and LiF 1A, LiF 2A, LiF 1B and LiF 2B covering the wavelength range 1000 - 1187 Å. *FUSE* observes through three apertures- LWRs, MDRS and HIRS with aperture size $30'' \times 30''$, $4'' \times 20''$ and $1.25'' \times 20''$ respectively. Here we use data from the LiF 1A segment since its sensitivity near 1032 Å is almost double to that of the other segments.

We obtained the calibrated data for the 69 sightlines analysed by Pathak et al. (2011) (see Table 1) from the Multi-mission Archive at STScI (MAST). These were processed by the latest *FUSE* data reduction pipeline CALFUSE V3.2 (Dixon et al. 2007). Out of the 69 sightlines, O VI absorption has already been reported for 1 sight line by Friedman et al. (2000); for 11 sightlines by Howk et al. (2002b); 3 by Danforth & Blair (2006); and 1 by Lehner & Howk (2007). Although the native *FUSE* resolution is 20 km s^{-1} in this region, we have uniformly downgraded all the spectra to a resolution of 35 km s^{-1} to have a higher signal-to-noise, irrespective of the quality of the original spectrum.

3.1 Continuum and Contamination

Our first task was to define a stellar continuum near the O VI profile for which we used Legendre polynomials as described by Sembach & Savage (1992) and Howk et al. (2002a). For most of the sightlines a low order polynomial (≤ 5) is enough to model the continuum, except for a few sightlines (e.g., Sk-67D05, Sk-67D168, Sk-70D115 etc.) that show complex behaviour. These sightlines show a sudden hike or trough near the O VI absorption. Polynomials of higher order (> 5) were required to fit such continuum. To measure the error in the continuum fitting we have tested two continua other than the assumed continuum, one just above and the other just below the real continuum giving 1σ significance level.

Another source of error in the O VI column density measurements is the contamination from Galactic and LMC molecular hydrogen. We modeled the H_2 absorption lines

that arise due to $6-0 \text{ P}(3)$ and $6-0 \text{ R}(4)$ transitions following Howk et al. (2002a) (Table 3). In this model we used the intensity of existing H_2 absorption lines that are not blended with other lines and use the ratio of the oscillator strengths. The model estimated the strength of the 1031.20 Å and 1032.35 Å H_2 line. These were subtracted from the O VI profiles that appear in the same wavelength region. This is not a major problem for the LMC absorption lines which are shifted to a higher velocity (Howk et al. (2002a); Pathak et al. (2011)) but may affect the Galactic O VI significantly. We have plotted a representative sample of normalized spectra of the O VI absorption at 1032 Å in Figure 1. HD lines were modeled but we find that these are extremely weak and their contribution is within the error bars of O VI.

Stellar wind variability and mass loss may add significant error in the O VI column density measurements. Interstellar O VI identification and stellar continuum placement is complicated because of stellar wind variability. Following Zsargó, Sembach & Howk (2003) we have selected by eye those the objects for which we had confidence in the continuum placement, line identification, and blending decontamination. Bowen et al. (2008) studied the absorption spectrum of HD 178487 in detail and estimated the uncertainty due to stellar mass loss to be about 0.1 dex.

3.2 Apparent Optical Depth Measurements

We have used the apparent optical depth (AOD) technique (Savage & Sembach 1991; Sembach & Savage 1992; Howk et al. 2002a) to measure the equivalent width and column density of the O VI absorption lines. This technique uses an apparent optical depth (τ_a) in terms of velocity defined as

$$\tau_a(v) = \ln[I_o(v)/I_{obs}(v)], \quad (1)$$

where I_o is the continuum intensity and I_{obs} the intensity of the absorption line in terms of velocity. This method is well suited for observations where the instrument is able to completely resolve the absorption line.

The apparent column density ($N_a(v)$ in units of atoms cm^{-2} (km s^{-1}) $^{-1}$) is calculated from the apparent optical depth using the expression

$$N_a(v) = \frac{m_e c \tau_a(v)}{\pi e^2 f \lambda} = 3.768 \times 10^{14} \frac{\tau_a(v)}{f \lambda}, \quad (2)$$

where m_e is the mass of the electron, c is the speed of light, e is the electronic charge, λ is the line wavelength (in Å) and f is the oscillator strength of the atomic species. For O VI, f value of 0.1325 has been taken from Yan et al. (1998). The O VI absorption is a doublet with absorptions at 1032 and 1038 Å. While the 1032 Å O VI profile is broad and is completely resolved by *FUSE*, the 1037.6 Å is difficult to separate from the CII* absorption line. Because of this we have only used the 1031.93 Å line in our analysis.

We have listed derived equivalent widths and column densities for O VI in Table 1. The 1σ error in the equivalent width and column density has been derived using the uncertainty in the *FUSE* data and the fitting procedures. Another major uncertainty is due to the overlap of high velocity MW O VI with that of the LMC absorption. The separation is distinct for some sightlines viz. Sk-65D21, Sk-67D69,

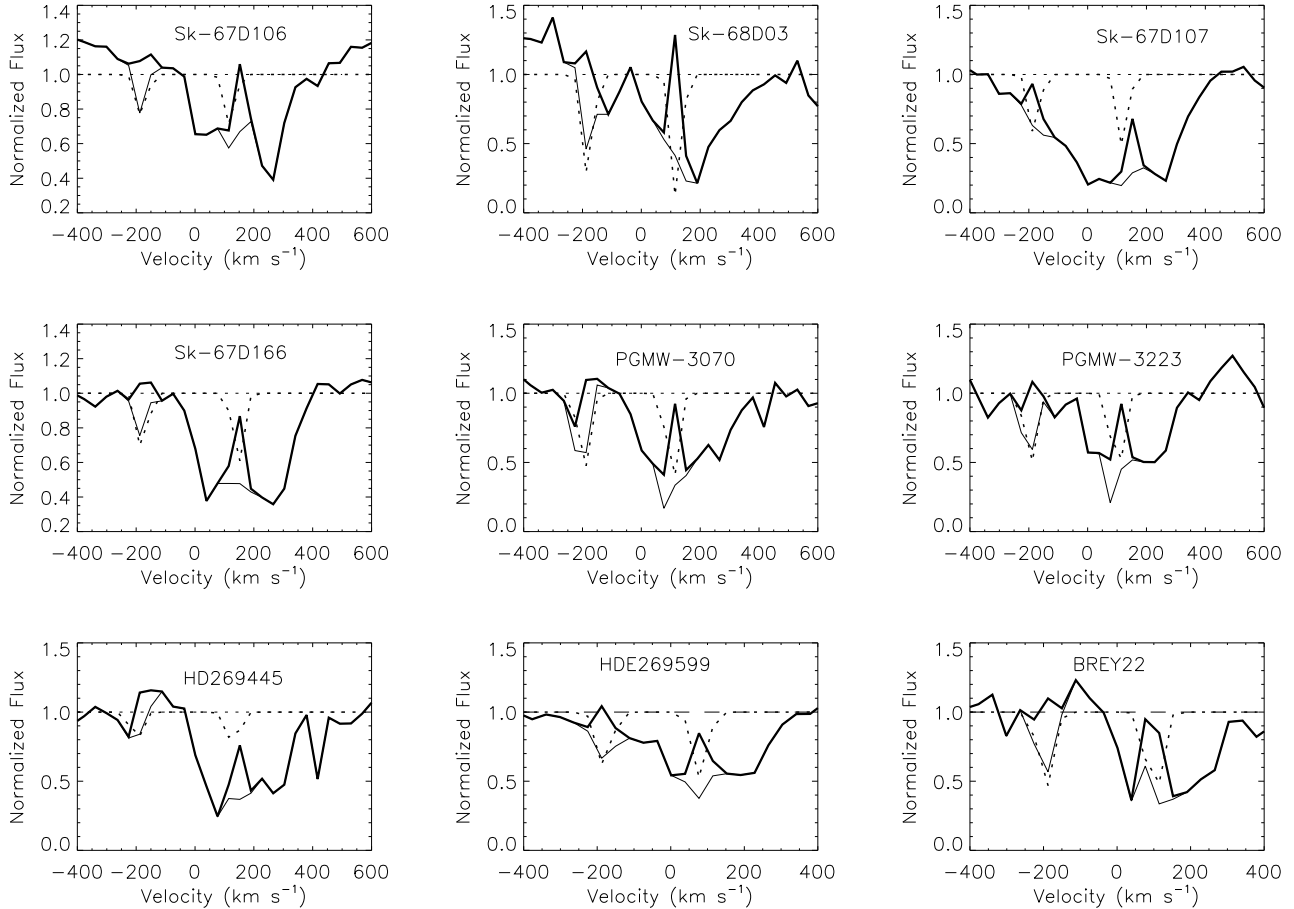


Figure 1. O VI absorption profiles for few lines of sight in the MW. Absorption line profiles of O VI before (gray line) and after (black line) removal of H₂ contamination are shown. Model for H₂ absorption (dotted line) for these lines of sight are also shown.

Sk-65D105, HV2543, Sk-66D100, HV5936, Sk-67D211, Sk-69D220, Sk-66D172, Sk-68D137 and D301-1005. For overlapping lines, the lower velocity limit of the LMC O VI absorption from Pathak et al. (2011) is taken as the upper limit of the MW O VI profile. The range of the velocity considered for the integration is presented in Table 1. The LMC results from Pathak et al. (2011) are also presented. The uncertainty in exactly resolving the velocity limits may lead to significant errors in the measurements of high velocity clouds (HVCs).

For understanding the distribution of O VI, we have tried to separate the O VI in the MW disk from the IVCs and HVCs. For this the velocity limits are chosen as $|v| \leq 50$ km s⁻¹ for the O VI in the MW disk, 50 to 100 km s⁻¹ for the O VI in the IVCs and $|v| \geq 100$ km s⁻¹ for the O VI in the HVCs. The results from these measurements are presented in Table 2.

4 CHARACTERISTICS OF O VI IN THE MW

4.1 Fe II absorption and kinematic properties of O VI

It is difficult to directly compare the kinematics of O VI in the MW and the LMC based only on the absorption profiles because the O VI profiles are broad (Figure 2) suggesting that they arise in an extended halo of hot gas. A better probe of the kinematics of the gas is the optically thin Fe II absorption line at 1125.448 (Howk et al. 2002b). These lines trace the low-ionization gas associated with the relatively high column density warm neutral medium (WNM) and warm ionized medium (WIM) and we observe two components, one at low negative velocities arising in the MW and the other at high positive velocities arising in the LMC (Figure 2; (Howk et al. 2002b)).

The O VI absorption in the MW is observed as a broad line at negative velocities (except for Sk-70D97, BI253 and HV982) arising in both the low velocity components tracked by the Fe II absorption line and in IVC and HVC components where no Fe II is seen.

Evidence of IVC and/or HVC components in the O VI absorption profiles for LMC can also be seen for all sight-lines. In comparison to Fe II, O VI absorption profiles in the

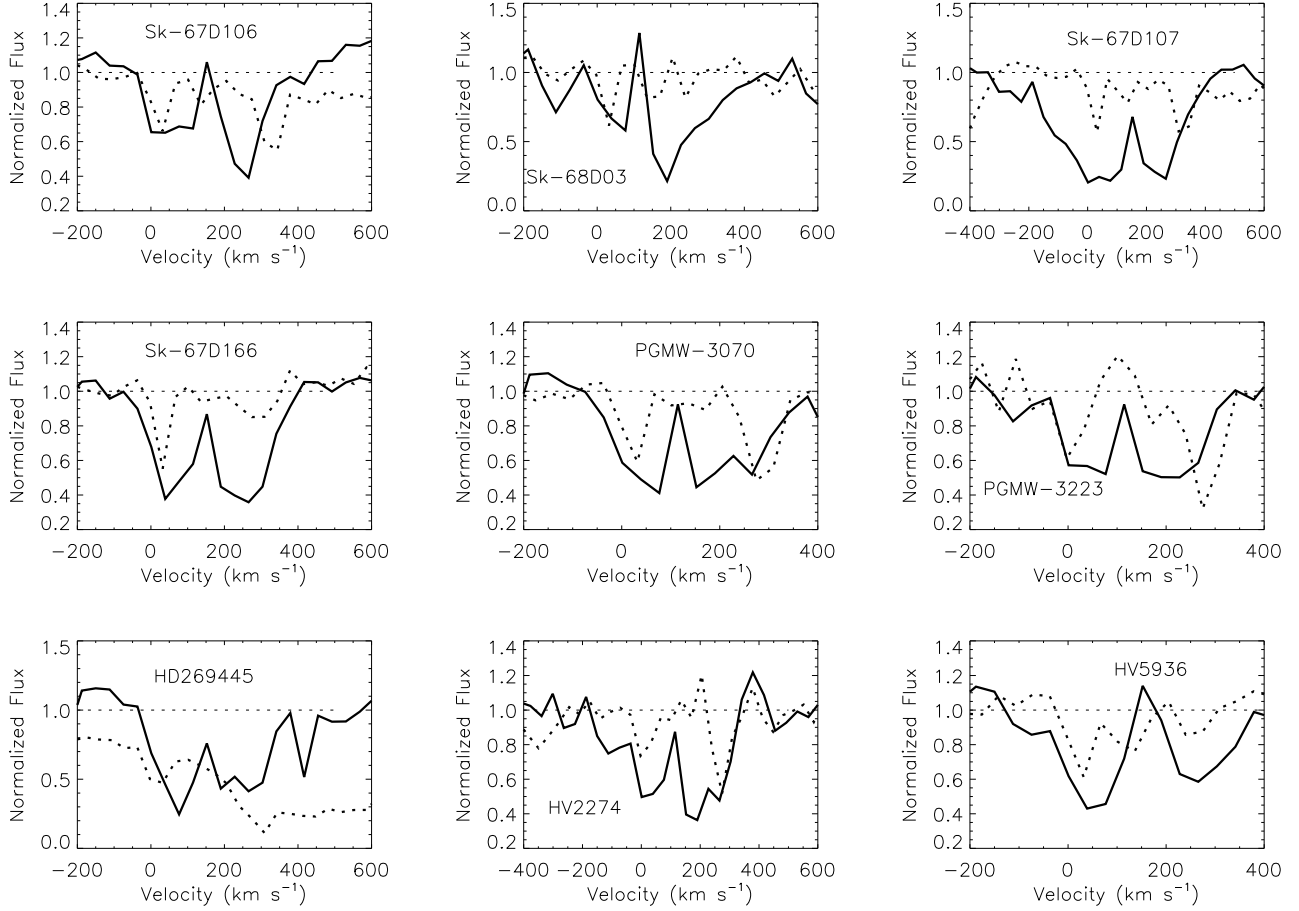


Figure 2. O VI absorption profiles (black lines) for few lines of sight along with Fe II components (dotted lines) in the MW and LMC. Significant absorption (probably stellar) for HD269445 (lower left panel) results in a shift of the continuum of the Fe II profile.

LMC extend to the lower velocities. Almost all Fe II profiles are aligned to the high velocity edge of O VI. Therefore, Fe II present in the LMC is close to the disk and O VI is an extended gas.

4.2 High velocity O VI

Absorption or emission spectra against bright extragalactic sources provide information about the large gaseous structures surrounding the MW. Gas with radial velocities $|V_{LSR}| > 100 \text{ km s}^{-1}$ are usually the HVC and IVC is considered to be the gas having velocities $50 < |V_{LSR}| < 100 \text{ km s}^{-1}$. HVCs are often described in terms of the HI 21 cm emission and connect the inner region of a galaxy with the surrounding intergalactic medium. Towards several HVCs, H α emission has been detected (Tuftes, Reynolds, & Haffner 1998; Bland-Hawthorn et al. 1998; Weiner & Williams 1996). UV spectra of bright extragalactic stars have revealed neutral, weakly, and highly ionized gas at high velocities (Savage & de Boer 1981; Welty, Frisch, Sonneborn, & York 1999; Lehner et al. 2001; Danforth et al. 2002; Hoopes et al. 2002; Howk et al. 2002b; Lehner 2002). The HVC has a complex multi-phase structure but the Hubble Space Tele-

scope and *FUSE* results have shown that some HVCs are almost fully ionized (Sembach et al. 1995, 1999; Putman et al. 2003; Lehner, Staveley-Smith & Howk 2009).

Most of the large IVCs and HVCs are located in the inner Galactic halo at distances $d \leq 20 \text{ kpc}$ (Wakker et al. 2007; 2008; Thom et al. 2006; 2008) except the “Magellanic Stream” (MS) which is at $\sim 50 \text{ kpc}$ (Gardiner & Noguchi 1996). The accretion of gas from the two Magellanic Clouds by the MW has been considered as the origin of Magellanic Stream (Wannier, & Wrixon 1972; Fox et al. 2010; 2013, 2014; Richter et al. 2013).

Other HVCs possibly represent metal-deficient gas that is infalling from the inter-galactic medium. Earlier a Galactic origin of the HVC towards the LMC was proposed (Savage & de Boer 1981; de Boer, Morras, & Bajaja 1990; Richter et al. 1999) while recent studies reveal energetic outflow from the LMC as the origin of the HVC complex (Lehner, Staveley-Smith & Howk 2009).

4.3 Doppler parameter

The width of an absorption line is a measure of the total velocity distribution in the gas which, in the case of Galactic lines, may be due to thermal motion, turbulence or multi-

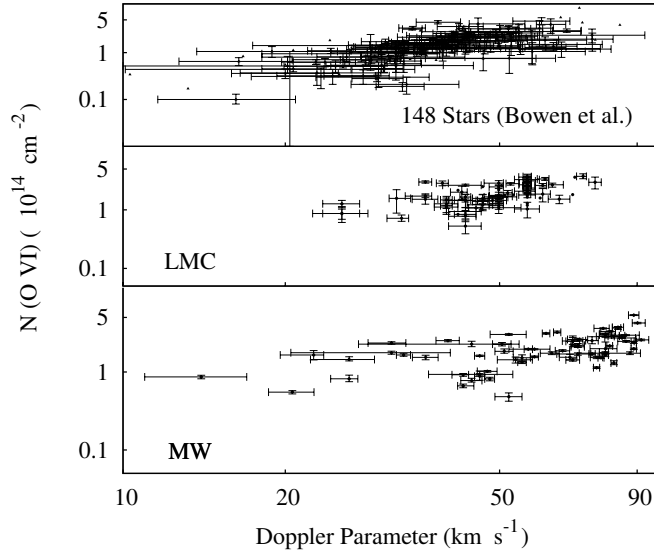


Figure 3. O VI column density $[N(\text{O VI})]$ vs Doppler parameter, b . Top panel shows the results obtained by Bowen et al. (2008). The lower panel represents our results derived for the 69 sightlines and the middle panel represents results for the same 69 sightlines for LMC obtained by Pathak et al. (2011)

ple components in the line of sight and is characterized by the Doppler parameter (b) where $b = \text{FWHM}/2\sqrt{\ln(2)}$. For high resolution observations such as those with *FUSE* where the O VI absorption line is fully resolved, the AOD method provides a direct measure of b . The b -value has further been corrected by subtracting the second moment for the smoothed line-spread function from the second moments of the observed profiles. The production of O VI in collisional ionization equilibrium (CIE) is maximum at 2.8×10^5 K (Sutherland & Dopita 1993). At this temperature the thermal Doppler line width should be 17.1 km s^{-1} corresponding to a FWHM of 28.5 km s^{-1} . The observed b value for all sightlines of this study ranges from $14.0^{+1}_{-1} \text{ km s}^{-1}$ for BREY22 to $91.6^{+2}_{-2} \text{ km s}^{-1}$ for HV5936. The corresponding median, average and standard deviation of Doppler parameter are 68.4 km s^{-1} , 62.7 km s^{-1} and 20.0 km s^{-1} respectively. The average b -value is larger than expected from thermal broadening in a gas at 2.8×10^5 K. This may be due to different environments dominated by inflow, outflow and turbulent motions.

For the MW O VI Savage et al. (2003) found $\langle b \rangle = 61 \pm 15 \text{ km s}^{-1}$ with a median value of 59 km s^{-1} for 100 extragalactic sightlines. Earlier Jenkins (1978a) found a variation in the value of b for the Galactic disk from 10.7 to 56 km s^{-1} with median value of 27 km s^{-1} for O VI absorption towards 62 stars observed by the *Copernicus* satellite. O VI velocity dispersions from 33 to 78 km s^{-1} with an average $\langle b \rangle = 45 \pm 11 \text{ km s}^{-1}$ was reported for 22 halo stars by Zsargó, Sembach & Howk (2003). Lehner et al. (2011) also derived the O VI b -distribution in the Milky Way disk and found a variation from 20 to 60 km s^{-1} .

The distribution of the Doppler parameter and the column density is used to understand the variation in the temperature and the density of the ISM. A linear correlation between $N(\text{O VI})$ and b was first discussed by Heckman et al.

(2002), who studied the trend using extragalactic sightlines and data from early investigations of O VI in the Galaxy. The discussed correlation between O VI column density and Doppler parameter is expected in radiatively cooled or conductively heated gas. This correlation extends from the local interstellar medium (LISM) to the Galactic disk and the halo and beyond (Heckman et al 2002; Savage et al. 2003). Bowen et al. (2008) found a similar relation in the Galactic disk for O VI. A good correlation between the Doppler parameter and the O VI column density for $b > 15 \text{ km s}^{-1}$ was reported by Lehner et al. (2011). In Figure 3 (bottom panel) we plot $N(\text{O VI})$ against Doppler parameter b . We find a correlation as reported in earlier studies. For comparison we also plot the results of Pathak et al. (2011) and Bowen et al. (2008) in the middle and upper panels respectively. O VI Doppler line width in the LMC is found to be confined in a narrower range compared to that of the MW. Heckman et al. (2002) suggested that the correlation depends on the characteristic velocity which may be explained by the laws of heating or cooling. The correlation suggests a collision dominated ionisation for O VI production (Lehner et al. 2011). In Figure 4, the histogram of the values of b for all the sightlines are shown. In the right panel of Figure 4 we also present the histogram of b values as obtained by Pathak et al. (2011) for the LMC. The histogram plots indicate that the b values are larger than the value for which maximum O VI is expected. Thus, the gas experiences nonthermal motion that dominates the broadening. There may also be undefined components contributing to the profile width (Lehner et al. 2011).

4.4 Column density

We find a variation of about an order of magnitude in the O VI column densities in the MW lying between 13.68 to

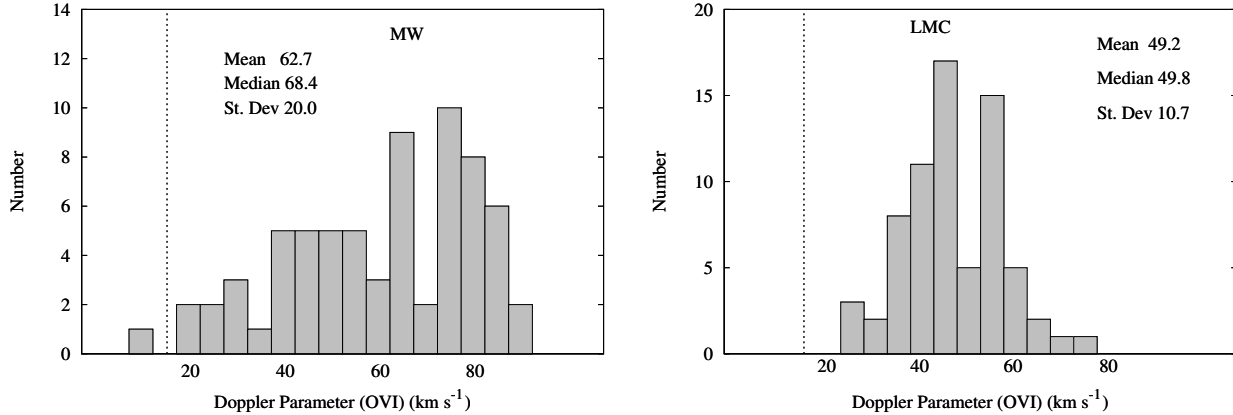


Figure 4. Doppler parameter distribution of O VI considering a bin size of 5 km s⁻¹ for the MW (left) and the LMC (right). The vertical dotted line represents the expected b-value at maximum O VI abundance temperature in CIE.

14.73 (in units of atoms cm⁻²) for log N(O VI). The mean MW O VI column density is found to be 14.26 atoms cm⁻² and the median value for our sample is 14.27 atoms cm⁻². The projections of the total column densities perpendicular to the Galactic plane, log (N sin |b|) are in approximately the same range: from 13.42 to 14.50 atoms cm⁻² with average and median values of 14.00 and 14.02 atoms cm⁻² respectively. Similar values of O VI column densities are reported in different literature as given in Table 3.

As discussed in section 4.1, the O VI profiles for all sightlines in our sample have HVC and/or IVC components. For the low velocity component, we have derived the MW O VI column densities by integrating over $|v| \leq 50$ km s⁻¹ (Table 2). This velocity range is nearly free from the IVC. The log N(O VI) for this velocity range varies from 12.55 to 14.52 atoms cm⁻². The mean column density log N(O VI) for this range is 13.94 atoms cm⁻².

The log N(O VI) for the velocity range $|v| \leq 100$ km s⁻¹ representing the disk with the IVC component, varies from 14.63 to 13.61 atoms cm⁻². The mean column density log N(O VI) for this range is 14.24 atoms cm⁻². There are 5 sightlines where the IVC contribution to the total O VI column density is greater than 70% and 14 sightlines where the contribution is $> 50\%$. Howk et al. (2002b) report O VI column density values in the Galactic halo from 13.61 to 14.23 atoms cm⁻² in the velocity range -50 to +50 km s⁻¹ and 14.22 to 14.67 atoms cm⁻² when integrated over total velocity range for 12 stars in the LMC. The individual sightline of the 12 stars have varying column density values for the two corresponding velocity limits.

Out of the 69 sightlines, we have not found HVC component in case of BREY22 and HDE269599 (Figure 1). Except these two, it is observed that the HVC contribution is significant for all other sightlines. For $|v| > 100$ km s⁻¹ region, log N(O VI) ranges from 9.78 to 14.03 atoms cm⁻² with a mean of 12.87 atoms cm⁻². There are 9 cases where the HVC contribution to the total column density is $\geq 20\%$. The highest contribution from this velocity range is found in case of Sk-71D45.

4.5 Comparison with the LMC and the SMC

The metallicity of the MW is higher than that of the LMC and the SMC with SMC being the lowest. This implies that the O VI abundance in the MW would be higher compared to that of the LMC and the SMC. O VI column density for all the 69 lines in the LMC have already been reported by Pathak et al. (2011). They found high abundance of O VI with log N(O VI) in the range of 13.72 to 14.57 atoms cm⁻² and a mean of 14.23 atoms cm⁻². The variation of column density in the LMC is lower than the MW. The mean O VI column density for the MW is higher than the LMC. Considering the inclination angle of the LMC to be 33°, Pathak et al. (2011) calculated the projected O VI column density on the plane as 14.16. Table 1 presents a comparison of the equivalent widths and the column densities in the two galaxies for all sightlines. We find that the O VI column densities in the MW are higher (or comparable) to the LMC values. The O VI absorption profiles are similar to that of the LMC which is in agreement with Pathak et al. (2011).

Howk et al. (2002a) analysed the distribution and kinematics of O VI absorption towards 12 early-type stars in the LMC. They observed O VI absorption for all 12 stars and derived column densities in the range of 13.9–14.6 atoms cm⁻² with a mean of 14.37 atoms cm⁻². They report that the average column density of O VI and the dispersion of the individual measurements about the mean are identical to those measured for the halo of the MW.

Since, the O VI absorption is very patchy in nature and the O VI abundance depends on the local ISM conditions, it is extremely difficult to compare the O VI column densities of the MW and the LMC.

O VI absorption in the SMC was surveyed by Hoopes et al. (2002) for 18 early-type stars. They report a widespread presence of O VI with a mean value of N(O VI) as 14.53 atoms cm⁻². While the metallicity of the SMC is lower, the mean column density is higher than the MW and the LMC. Highest abundance of O VI has been found for NGC 346 which is a star forming region of the SMC. In the SMC the O VI profile is shifted to higher velocities compared to the lower ionization gas traced by Fe II absorption (Hoopes et al. 2002).

4.6 O VI column density and angular variation

The O VI column densities have been measured using AOD method for 69 stars in the LMC [(l,b)=280°.5, - 32°.9 and d= 50 kpc]. As evident from Table 1, there exists significant variation in the N(O VI) values. The lowest value of column density has been found to be 4.82×10^{13} atoms cm^{-2} for SK-65D63. For LH91486 the value is highest which is 5.36×10^{14} atoms cm^{-2} . This gives a variation of about one order of magnitude.

The column density variation with respect to the angular scale may provide us information on physical properties of the regions in which O VI is produced. An idea of the physical dimension and shape of the O VI bearing clouds may be obtained from the amount of change in N(O VI) and angular scale variations. Though uniform distribution of hot gas in the galactic halo was considered (Spitzer 1956), soon it became clear that the O VI distribution is not smooth in the galaxy (Savage et al. 2003). Howk et al. (2002b) found large variations in the MW O VI column densities over small angular scales towards 12 LMC and 11 SMC stars. They found column density variations for the smallest scales with a value of $\Delta\theta \sim 1'.8$. No significant N(O VI) variation was found towards 4 stars in NGC 6752 that are separated by $2'.2 - 8'.9$ (Lehner & Howk 2004).

The sightlines in our study are separated by angular distances of $0.0025^\circ \leq \Delta\theta \leq 6.35^\circ$. The smallest scale for which O VI column density variation has been measured is $\Delta\theta \sim 0.0025^\circ$ for the closest pairing stars Sk-69D243 and MK42. On the other hand Sk-65D21 and Sk-68D03 are found to be the most distant lines of sight ($\Delta\theta \sim 6.35^\circ$). Assuming O VI absorption by HVCs located in the halo of the Galaxy towards the LMC at a distance of 40 kpc from the Sun (Lehner, Staveley-Smith & Howk (2009); Sarma et al. (2014)), we find the distance between the closest and most distant stars to be 1.75 pc and 4.43 kpc respectively. Figure 5 shows the difference in column densities for each pair of sightlines versus the angular separation of the pair. We measure absolute column density difference i.e. $\Delta N(\text{O VI}) = N(\text{O VI})_i - N(\text{O VI})_j$ for each pair of sightlines i and j. In Figure 5 we show relative variation in $\Delta N(\text{O VI})$ for object pairs plotted against the angular separation of the pair. There exists clear variation in the amount of N(O VI) over all angular scales. The average and standard deviation of logarithmic values of column density difference of each sightline is found to be 13.83 and 0.49 atoms cm^{-2} . This result confirms the patchiness of O VI in the Galaxy.

Following Howk et. al (2002b), we also derived the angular autocorrelation function (ACF) $w(\theta)$ for O VI column densities towards all the 69 sightlines. The ACF is calculated using the expression

$$w(\theta) = \frac{\sum_i \sum_{j \neq i} (N_i - \langle N \rangle)(N_j - \langle N \rangle)(\sigma_i \sigma_j)^{-1}}{\langle N \rangle^2 \sum_i \sum_{j \neq i} (\sigma_i \sigma_j)^{-1}}, \quad (3)$$

where N_i and N_j are the O VI column densities with uncertainties σ_i and σ_j . This is the same expression as Howk et. al (2002b) used except that the weight factors have been raised to (-1).

The average column density of 69 sightlines is represented by $\langle N \rangle$. We have considered the bin spacing as 0.2° for the whole data set. The derived values of $w(\theta)$ are shown in Figure 6.

We find significant variation of $w(\theta)$ on small scales. Below 2° , the maximum factor by which the ACF varies is ~ 1.6 . This indicates that the cloud structure may be much smaller. At large scales, the variation of $w(\theta)$ is not significant (~ 0) which is similar to the earlier result (Howk et al. 2002b).

Howk et al. (2002b) discuss the angular correlation function of the O VI measurements, finding no preferred angular scale for variations. Savage et al. (2003) showed that the variation seen towards the LMC and the SMC extend to larger angular scales. They favoured models in which the O VI-bearing medium is composed of small complex cloud-like or sheet-like distribution of material (Howk et al. 2002b; Savage et al. 2003).

4.7 Scale Height

Another aim of this work is to study the distribution of O VI in the Galactic plane with a large sample size compared to earlier studies (Jenkins (1978b); Savage et al. (2003); Bowen et al. (2008); Savage & Wakker (2009)). We assume an exponential gas distribution with O VI volume density as a function of height (z), $[n(|z|)=n_0 \exp(-|z|/h)]$ where h is scale height and n_0 is midplane density]. The column density N(x) perpendicular to the plane for an object with latitude b is given by $N(x) \sin |b|=n_0 h [1-\exp(-|z|/h)]$, where $N(x) \sin |b|$ is the line-of-sight column density of an object. For extra-galactic objects ($|z| \gg h$), $N(x) \sin |b|=n_0 h$ is used.

Using *Copernicus* data the midplane density n_0 and corresponding O VI scale height have been estimated to be $2.8 \times 10^{-8} \text{ cm}^{-3}$ and 0.3 kpc respectively by Jenkins (1978b). The *Copernicus* O VI observations have been reanalyzed by Shelton & Cox (1994) and they found that the midplane O VI density beyond the Local Bubble (LB) is $(1.3 - 1.5) \times 10^{-8} \text{ cm}^{-3}$ for an O VI absorbing layer with $h \sim 3$ kpc. Savage et al. (2000) estimate $n_0 = 2.0 \times 10^{-8} \text{ cm}^{-3}$ from *Copernicus* O VI survey and derived scale height $h > 2$ kpc. Using *FUSE* data of 100 extragalactic objects Savage et al. (2003) derived a scale height of $h \sim 2.5$ kpc. Bowen et al. (2008) used *FUSE* data of 148 early type stars and estimated midplane density $n_0 = 1.33 \times 10^{-8} \text{ cm}^{-3}$ which decreases away from the plane of the Galaxy. Bowen et al. (2008) considered a correction for O VI absorption in the LB and measured O VI scale height as 3.2 kpc at negative latitudes or 4.6 kpc at positive latitudes.

We measure the scale height for all the sightlines of our study. For a midplane density $n_0 = 1.64 \times 10^{-8} \text{ cm}^{-3}$ (Savage & Wakker 2009), we obtain the scale height using the simple relation $h = N(x) \sin |b| / n_0$. The value ranges from 0.53 to 6.4 kpc. The average values of the O VI scale height is 2.28 ± 1.06 kpc. Savage & Wakker (2009) using a large object sample (109 stars and 30 extragalactic objects) derived the O VI scale height to be 2.6 ± 0.5 kpc from the Galactic plane. We have also calculated the scale height for all the sightlines for the column density derived in the range from minimum to 100 kms^{-1} . The average scale height in this case has been found to be 2.05 kpc.

From the O VI scale height value, the temperature of the ionized plasma can be found as estimated by Savage & Wakker (2009). Considering hydrostatic equilibrium at temperature T for an isothermal gas, the scale height is given by $h = kT / (m)g(|z|)$. The value of gravitational acceleration

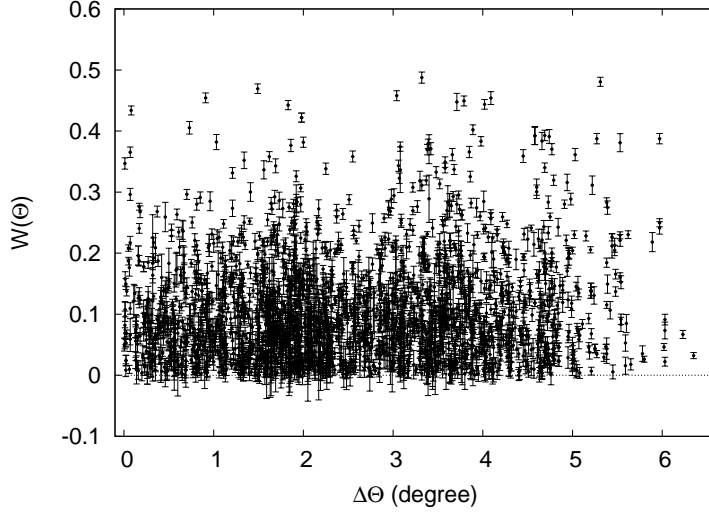


Figure 5. Absolute logarithmic column density difference, $\Delta N(\text{O VI}) = N(\text{O VI})_i - N(\text{O VI})_j$ for each (ij) pair of sightlines as a function of angular separation between the pairs.

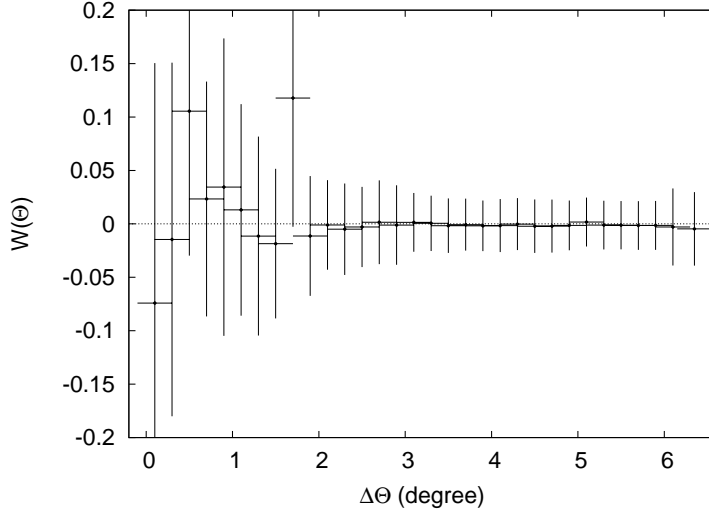


Figure 6. Autocorrelation function, $w(\theta)$ vs Angular separation for the 69 sightlines considering 0.2° bin spacing. We consider the binsize and standard deviation as the error for $\Delta(\theta)$ and $w(\theta)$ respectively.

towards the disk $g(|z|)$, in the solar neighbourhood for a distance 1-10 kpc is $\sim 10^{-8} \text{ cm s}^{-2}$ (Kalberla & Dedes 2008). Considering average mass per particle $\langle m \rangle = 0.73 m_H$, for a scale height $h = 2.28$ kpc the temperature of the gas is found to be $T \sim 0.62 \times 10^6$ K. This temperature is ~ 2.21 times larger than the transition temperature of O VI. Savage & Wakker (2009) derived this temperature as $\sim 0.8 \times 10^6$ K for a scale height value $h = 3$ kpc.

5 SUMMARY AND CONCLUSION

We have studied the properties of O VI in the MW along the lines of sight towards 69 stars in the LMC using *FUSE* spectra. The observed absorption lines are studied using AOD method which reveal significant variation in O VI column densities over small angular scale. The important results of these study may be summarized as follows:

1. We find O VI absorption in the MW with IVC and HVC components. The highest column density measured for the MW is $\log N(\text{OVI}) = 14.73$ atoms cm^{-2} and the minimum value is $\log N(\text{OVI}) = 13.68$ atoms cm^{-2} . The mean MW O VI column density is found to be 14.26 atoms cm^{-2} . The median value of our sample is 14.27 atoms cm^{-2} . The logarithm of the column densities perpendicular to the Galactic plane varies between 13.42 and 14.50 atoms cm^{-2} with an average value of 14.00 atoms cm^{-2} . We observed the O VI absorption line at 1036 \AA but did not use it as it overlaps with the CII* absorption line.

2. There is a significant variation in the O VI column densities on all scales ($0.0025^\circ - 6.35^\circ$). Higher variation towards smaller angular scale indicates that the O VI bearing clouds are small in size.

3. The measured O VI column densities can be described by a patchy exponential distribution in the MW which is in

accordance with earlier measurements of O VI absorption for the Galaxy.

4. The velocity dispersion (b -values) of the O VI absorption profiles range from 14.0 to 91.6 km s⁻¹. The median, average and standard deviation of equivalent width are 68.4, 62.7 and 20.0 km s⁻¹ respectively. The average b -value is larger than expected from thermal broadening in gas at 2.8×10^5 K. This may be due to different environments dominated by inflow, outflow and turbulent motions.

5. The broad (>25.24 km s⁻¹) O VI absorption profiles suggest collisional ionization at the interface of warm-hot ISM to be the mechanism that produces this ion.

6. The O VI column density and the Doppler parameter, b , are found to be correlated for our sample of sightlines. This confirms earlier results.

7. A kinematical comparison of Fe II and O VI line profiles reveal the presence of HVC and/or IVC components in the O VI absorption along all sightlines. In the Fe II profiles we have not observed either of these components. The distribution of O VI is significantly different than that of Fe II. The broad absorption profiles of O VI trace extended layers compared to that of the Fe II-bearing layer.

8. For a midplane density $n_0 = 1.64 \times 10^{-8}$ cm⁻³, we measured the O VI scale height as 2.28 ± 1.06 kpc. This is in accordance with earlier results.

A thorough mapping of O VI in the MW and in nearby galaxies will be helpful in understanding the distribution and kinematics of the ionized gas. Future scientific mission which may cover O VI wavelengths will definitely explore much more about the hot ionized phase of the ISM.

Table 1: O VI column densities, equivalent widths and the corresponding velocity limits in the Milky Way and the LMC.

Target Name	Limit (km s ⁻¹)	Milky Way EW (mÅ)	log N(O VI) (dex)	Limit (km s ⁻¹)	LMC EW (mÅ)	log N(OVI) (dex)
SK-67D05	-30,175	259.9±15	14.26 ^{+0.03} _{-0.03}	175, 330	73±6	13.72 ^{+0.10} _{-0.13}
SK-68D03	-20,120	122±18	14.06 ^{+0.04} _{-0.04}	180,330	112±8	14.02 ^{+0.11} _{-0.15}
BI13	-35,120	190.0±27	14.25 ^{+0.06} _{-0.08}	175, 315	88±4	13.94 ^{+0.08} _{-0.09}
SK-67D18	-30,135	130.3±17	14.12 ^{+0.13} _{-0.16}	165, 330	132±7	14.16 ^{+0.09} _{-0.13}
Sk-67D20	-30,175	200.2±3	14.19 ^{+0.06} _{-0.07}	175, 335	147±8	14.08 ^{+0.11} _{-0.16}
PGMW-3070	-50,120	139.2±15	14.23 ^{+0.12} _{-0.16}	180, 345	132±23	14.10 ^{+0.13} _{-0.18}
LH103102	-20,150	287.0±23	14.38 ^{+0.02} _{-0.03}	180, 330	132±23	14.16 ^{+0.03} _{-0.04}
LH91486	-30,175	459.9±22	14.73 ^{+0.05} _{-0.06}	175, 385	266±29	14.47 ^{+0.09} _{-0.11}
PGMW-3223	-50,120	138.9±17	14.01 ^{+0.06} _{-0.07}	175, 315	129±15	14.10 ^{+0.06} _{-0.07}
HV2241	-35,165	330.0±66	14.56 ^{+0.05} _{-0.06}	165, 365	271±18	14.50 ^{+0.04} _{-0.03}
HD32402	-40,140	253.5±22	14.40 ^{+0.08} _{-0.09}	160, 320	271±8	14.48 ^{+0.02} _{-0.02}
SK-67D32	-40,165	192.0±28	13.82 ^{+0.09} _{-0.11}	165, 360	129±7	14.11 ^{+0.03} _{-0.04}
SK-65D21	-20,165	111.0±29	13.91 ^{+0.08} _{-0.09}	225, 340	94±23	13.94 ^{+0.11} _{-0.16}
HV2274	-20,125	219.0±20	14.19 ^{+0.09} _{-0.11}	165, 345	160±11	14.14 ^{+0.10} _{-0.15}
Sk-66D51	-30,170	391.8±21	14.47 ^{+0.03} _{-0.02}	170, 370	185±10	14.26 ^{+0.01} _{-0.02}
NGC1818-D1	-50,150	320±20	14.46 ^{+0.03} _{-0.04}	150, 340	280±13	14.52 ^{+0.05} _{-0.05}
SK-70D69	-50,150	115.0±56	13.96 ^{+0.13} _{-0.19}	150, 295	182±12	14.18 ^{+0.07} _{-0.08}
Sk-67D69	-20,170	138.0±18	13.97 ^{+0.07} _{-0.10}	170, 340	232±28	14.40 ^{+0.05} _{-0.06}
MACHO78-6097	-30,165	236.9±50	14.32 ^{+0.05} _{-0.05}	165, 320	151±25	14.15 ^{+0.05} _{-0.05}
BI130	-30,165	339.9±6	14.39 ^{+0.11} _{-0.12}	165, 320	94±7	13.89 ^{+0.07} _{-0.09}
SK-69D94	-20,160	149.8±8	14.22 ^{+0.06} _{-0.06}	160, 340	150±3	14.22 ^{+0.03} _{-0.03}
SNR0519-697	2,160	339.0±16	14.44 ^{+0.05} _{-0.06}	160, 300	97±4	13.97 ^{+0.07} _{-0.08}
BREY22	10,160	105.6±20	13.94 ^{+0.08} _{-0.10}	160, 330	126±24	14.07 ^{+0.06} _{-0.07}
HD269445	-30,175	301.2±31	14.49 ^{+0.02} _{-0.02}	175, 365	200±10	14.29 ^{+0.04} _{-0.05}
SK-69D124	-35,190	136.4±26	13.95 ^{+0.10} _{-0.10}	190, 430	331±8	14.57 ^{+0.04} _{-0.05}
SK-67D105	-40,180	311.3±40	14.42 ^{+0.05} _{-0.05}	180, 320	110±8	13.92 ^{+0.14} _{-0.23}
SK-67D106	-20,150	113.0±22	13.89 ^{+0.08} _{-0.09}	175, 345	180±7	14.30 ^{+0.10} _{-0.13}
SK-67D107	-40,120	427.6±2	14.63 ^{+0.03} _{-0.03}	160, 360	254±10	14.45 ^{+0.04} _{-0.05}
HD36521	-30,175	190.0±3	14.24 ^{+0.13} _{-0.19}	175, 340	126±9	14.07 ^{+0.09} _{-0.12}
SK-68D82	-20,165	226.6±12	14.30 ^{+0.08} _{-0.09}	165, 320	141±10	14.17 ^{+0.04} _{-0.04}
BI170	-35,165	190.0±59	14.23 ^{+0.03} _{-0.03}	165, 365	235±20	14.43 ^{+0.02} _{-0.03}
SK-67D111	-30,175	260.0±10	14.46 ^{+0.05} _{-0.05}	175, 365	214±19	14.34 ^{+0.05} _{-0.05}
HV2543	-35,160	255.6±25	14.30 ^{+0.10} _{-0.09}	160, 365	156±42	14.23 ^{+0.04} _{-0.03}
SK-70D91	-45,160	243.0±20	14.39 ^{+0.04} _{-0.04}	160, 365	256±7	14.43 ^{+0.04} _{-0.03}
SK-66D100	-35,160	222.0±64	14.21 ^{+0.04} _{-0.05}	160, 340	214±21	14.34 ^{+0.03} _{-0.03}
HDE269599	-40,100	169.6±21	14.18 ^{+0.05} _{-0.05}	165, 320	123±6	14.05 ^{+0.03} _{-0.03}
SK-65D63	-40,150	54.0±19	13.68 ^{+0.16} _{-0.26}	180, 375	184±8	14.21 ^{+0.04} _{-0.04}
HV982	40,175	117.5±55	13.91 ^{+0.09} _{-0.09}	175, 360	208±58	14.33 ^{+0.12} _{-0.17}
SK-70D97	20,175	74.9±12	13.74 ^{+0.10} _{-0.12}	175, 375	226±4	14.39 ^{+0.03} _{-0.04}
Sk-67D144	-30,165	185.2±76	14.19 ^{+0.06} _{-0.07}	165, 335	194±10	14.25 ^{+0.06} _{-0.07}
BI184	-30,165	295.4±28	14.51 ^{+0.04} _{-0.04}	165, 330	118±10	14.04 ^{+0.08} _{-0.10}
NGC2004-B15	-30,165	200.5±24	14.22 ^{+0.09} _{-0.12}	175, 330	92±7	13.86 ^{+0.05} _{-0.07}
SK-71D38	-50,165	350.1±21	14.52 ^{+0.04} _{-0.04}	165, 315	94±7	13.92 ^{+0.07} _{-0.08}
Sk-71D45	-30,160	203.0±12	14.19 ^{+0.05} _{-0.06}	160, 345	194±9	14.26 ^{+0.06} _{-0.06}
SK-67D166	-20,165	260.0±21	14.29 ^{+0.04} _{-0.04}	165, 390	206±9	14.32 ^{+0.05} _{-0.05}
SK-67D168	-30,165	149.2±40	14.27 ^{+0.03} _{-0.02}	165, 375	186±12	14.26 ^{+0.05} _{-0.05}
SNR0532-675	-70,165	292.0±80	14.50 ^{+0.02} _{-0.02}	165, 345	147±9	14.16 ^{+0.07} _{-0.08}
SK-67D191	-40,165	462.7±27	14.64 ^{+0.01} _{-0.01}	165, 340	229±16	14.42 ^{+0.02} _{-0.02}
HV5936	-30,175	286.0±25	14.41 ^{+0.04} _{-0.05}	175, 375	174±8	14.18 ^{+0.07} _{-0.08}
SK-69D191	-30,165	219.0±41	14.22 ^{+0.04} _{-0.04}	165, 340	185±25	14.22 ^{+0.06} _{-0.07}
J053441-693139	-35,165	189.7±63	14.18 ^{+0.16} _{-0.24}	165, 330	182±33	14.22 ^{+0.05} _{-0.05}
Sk-67D211	-40,160	222.0±55	14.13 ^{+0.05} _{-0.07}	160, 350	144±8	14.11 ^{+0.10} _{-0.13}
BREY64	10,180	239.0±43	14.25 ^{+0.07} _{-0.25}	180, 330	139±8	14.20 ^{+0.16} _{-0.23}
SNR0536-692	38, 165	139.7±39.7	14.16 ^{+0.56} _{-0.24}	165, 320	116±7	14.03 ^{+0.07} _{-0.05}
SK-69D220	-40,155	222.0±23	14.33 ^{+0.02} _{-0.03}	160, 315	128±9	14.09 ^{+0.08} _{-0.11}
Sk-66D172	-30,175	316.9±38	14.47 ^{+0.03} _{-0.03}	175, 360	173±9	14.20 ^{+0.05} _{-0.05}
BI253	-20,160	260.0±46	14.36 ^{+0.04} _{-0.05}	160, 300	259±46	14.46 ^{+0.04} _{-0.05}
SK-68D137	-20,165	307.0±51	14.37 ^{+0.05} _{-0.06}	165, 330	234±7	14.45 ^{+0.03} _{-0.02}
MK42	-20,160	367.4±12	14.48 ^{+0.09} _{-0.11}	160, 330	228±24	14.41 ^{+0.07} _{-0.08}
SK-69D243	10,150	293.2±15	14.40 ^{+0.08} _{-0.09}	150, 345	307±15	14.56 ^{+0.05} _{-0.06}
30DOR-S-R136	-30,165	212.8±45	14.16 ^{+0.12} _{-0.13}	165, 320	185±25	14.25 ^{+0.05} _{-0.06}
SK-69D246	-40,145	358.9±2	14.56 ^{+0.03} _{-0.03}	155, 325	211±7	14.37 ^{+0.03} _{-0.03}
HDE269927	-40,160	228.6±21	14.34 ^{+0.06} _{-0.07}	160, 320	245±8	14.42 ^{+0.03} _{-0.04}
SK-69D257	-40,160	245.8±98	14.49 ^{+0.05} _{-0.06}	160, 315	171±8	14.20 ^{+0.07} _{-0.08}
SNR0543-689	0, 160	238.8±8.47	14.24 ^{+0.10} _{-0.08}	160, 360	186±34	14.27 ^{+0.10} _{-0.12}
D301-1005	-30,165	279.8±72	14.47 ^{+0.04} _{-0.05}	165, 385	284±57	14.53 ^{+0.02} _{-0.03}

FAR ULTRAVIOLET SPECTROSCOPIC EXPLORER OBSERVATION OF O VI ABSORPTION IN THE MILKY WAY

Table 1 – Continued

Target Name	Limit (km s ⁻¹)	Milky Way EW (mÅ)	log N(O VI) (dex)	Limit (km s ⁻¹)	LMC EW (mÅ)	log N(OVI) (dex)
SK-67D250	-40,165	212.8±58	14.29 ^{+0.04} _{-0.05}	165, 375	316±33	14.57 ^{+0.03} _{-0.03}
D301-NW8	-30, 175	204.2±35.5	14.15 ^{+0.02} _{-0.02}	175, 365	228±30	14.42 ^{+0.02} _{-0.03}
SK-70D115	-40,165	170.8±1	14.36 ^{+0.15} _{-0.23}	165, 330	186±11	14.23 ^{+0.03} _{-0.04}

Notes. LMC values are taken from Pathak et al. (2011)

Table 2: O VI column densities with the corresponding velocity limits in the Milky Way.

Target name	limit (km s ⁻¹)	log N(O VI) (dex)	limit (km s ⁻¹)	log N(O VI) (dex)	log N(O VI) [†] (dex)
SK-67D05	-30, 50	13.59 ^{+0.06} _{-0.08}	-30, 100	14.19 ^{+0.03} _{-0.03}	13.43 ^{+0.18} _{-0.12}
SK-68D03	-20, 50	13.74 ^{+0.07} _{-0.06}	-20, 100	14.03 ^{+0.01} _{-0.01}	12.81 ^{+0.18} _{-0.13}
BI13	-35, 50	14.02 ^{+0.07} _{-0.06}	-35, 100	14.23 ^{+0.06} _{-0.07}	12.97 ^{+0.21} _{-0.08}
SK-67D18	-30, 50	13.92 ^{+0.16} _{-0.11}	-30, 100	14.09 ^{+0.12} _{-0.17}	12.83 ^{+0.27} _{-0.02}
SK-67D20	-30, 50	13.63 ^{+0.10} _{-0.07}	-30, 100	14.05 ^{+0.07} _{-0.09}	13.61 ^{+0.22} _{-0.07}
PGMW-3070	-50, 50	14.09 ^{+0.16} _{-0.11}	-50, 100	14.22 ^{+0.12} _{-0.16}	12.51 ^{+0.27} _{-0.01}
LH103102	-20, 50	14.18 ^{+0.01} _{-0.01}	-20, 100	14.35 ^{+0.02} _{-0.02}	13.26 ^{+0.17} _{-0.13}
LH91486	-30, 50	14.31 ^{+0.06} _{-0.05}	-30, 100	14.63 ^{+0.05} _{-0.06}	14.03 ^{+0.20} _{-0.09}
PGMW-3223	-50, 50	13.98 ^{+0.08} _{-0.06}	-50, 100	14.01 ^{+0.06} _{-0.07}	10.06 ^{+0.21} _{-0.08}
HV2241	-35, 50	14.31 ^{+0.05} _{-0.04}	-35, 100	14.52 ^{+0.05} _{-0.05}	13.53 ^{+0.20} _{-0.10}
HD32402	-40, 50	14.17 ^{+0.06} _{-0.05}	-40, 100	14.36 ^{+0.07} _{-0.08}	13.29 ^{+0.07} _{-0.23}
SK-67D32	-40, 50	13.79 ^{+0.10} _{-0.08}	-40, 100	13.82 ^{+0.09} _{-0.11}	10.10 ^{+0.04} _{-0.24}
SK-65D21	-20, 50	13.67 ^{+0.09} _{-0.07}	-20, 100	13.90 ^{+0.07} _{-0.09}	12.14 ^{+0.23} _{-0.06}
HV2274	-20, 50	14.07 ^{+0.10} _{-0.08}	-20, 100	14.18 ^{+0.10} _{-0.12}	12.43 ^{+0.24} _{-0.04}
SK-66D51	-30, 50	13.83 ^{+0.03} _{-0.03}	-30, 100	14.37 ^{+0.01} _{-0.01}	14.02 ^{+0.17} _{-0.14}
NGC1818-D1	-50, 50	14.36 ^{+0.03} _{-0.03}	-50, 100	14.45 ^{+0.03} _{-0.03}	12.69 ^{+0.18} _{-0.12}
SK-70D69	-50, 50	13.66 ^{+0.02} _{-0.15}	-50, 100	13.96 ^{+0.13} _{-0.19}	11.63 ^{+0.04} _{-0.28}
SK-67D69	-20, 50	13.94 ^{+0.09} _{-0.07}	-20, 100	13.97 ^{+0.08} _{-0.09}	10.28 ^{+0.06} _{-0.28}
MACHO78-6097	-30, 50	14.04 ^{+0.05} _{-0.05}	-30, 100	14.29 ^{+0.05} _{-0.05}	13.21 ^{+0.20} _{-0.10}
BI130	-30, 50	14.09 ^{+0.05} _{-0.04}	-30, 100	14.28 ^{+0.08} _{-0.12}	13.73 ^{+0.03} _{-0.25}
SK-69D94	-20, 50	13.73 ^{+0.04} _{-0.03}	-20, 100	14.12 ^{+0.06} _{-0.07}	13.53 ^{+0.21} _{-0.09}
SNR0519-697	2, 50	14.05 ^{+0.06} _{-0.05}	2, 100	14.36 ^{+0.05} _{-0.06}	13.63 ^{+0.20} _{-0.09}
BREY22	10, 50	13.85 ^{+0.09} _{-0.08}	10, 100	13.94 ^{+0.08} _{-0.10}	-0-
HD269445	-30, 50	13.71 ^{+0.06} _{-0.04}	-30, 100	14.36 ^{+0.02} _{-0.03}	13.93 ^{+0.17} _{-0.13}
SK-69D124	-35, 50	13.34 ^{+0.09} _{-0.09}	-35, 100	13.85 ^{+0.08} _{-0.10}	13.24 ^{+0.23} _{-0.05}
SK-67D105	-40, 50	14.17 ^{+0.05} _{-0.05}	-40, 100	14.39 ^{+0.05} _{-0.05}	13.20 ^{+0.20} _{-0.10}
SK-67D106	-20, 50	13.79 ^{+0.23} _{-0.14}	-20, 100	13.81 ^{+0.15} _{-0.22}	10.05 ^{+0.02} _{-0.27}
SK-67D107	-40, 50	14.52 ^{+0.03} _{-0.02}	-40, 100	14.62 ^{+0.03} _{-0.03}	12.94 ^{+0.18} _{-0.12}
HD36521	-30, 50	14.06 ^{+0.17} _{-0.12}	-30, 100	14.19 ^{+0.13} _{-0.19}	13.31 ^{+0.28} _{-0.04}
SK-68D82	-20, 50	13.97 ^{+0.10} _{-0.07}	-20, 100	14.23 ^{+0.07} _{-0.09}	13.46 ^{+0.23} _{-0.06}
BI170	-35, 50	13.94 ^{+0.03} _{-0.02}	-35, 100	14.19 ^{+0.02} _{-0.02}	13.14 ^{+0.13} _{-0.18}
SK-67D111	-30, 50	14.29 ^{+0.05} _{-0.04}	-30, 100	14.43 ^{+0.05} _{-0.05}	13.20 ^{+0.20} _{-0.10}
HV2543	-35, 50	14.10 ^{+0.03} _{-0.03}	-35, 100	14.27 ^{+0.06} _{-0.08}	13.12 ^{+0.24} _{-0.07}
SK-70D91	-45, 50	14.11 ^{+0.04} _{-0.04}	-45, 100	14.34 ^{+0.03} _{-0.04}	13.46 ^{+0.19} _{-0.11}
SK-66D100	-35, 50	14.19 ^{+0.05} _{-0.04}	-35, 100	14.21 ^{+0.04} _{-0.05}	10.11 ^{+0.10} _{-0.19}
HDE269599	-40, 50	14.08 ^{+0.04} _{-0.04}	-40, 100	14.18 ^{+0.04} _{-0.05}	-0-
SK-65D63	-40, 50	13.16 ^{+0.41} _{-0.23}	-40, 100	13.61 ^{+0.16} _{-0.37}	12.90 ^{+0.33} _{-0.16}
HV982	40, 50	12.55 ^{+0.10} _{-0.08}	40, 100	13.86 ^{+0.07} _{-0.08}	12.97 ^{+0.22} _{-0.06}
SK-70D97	20, 50	12.91 ^{+0.16} _{-0.11}	20, 100	13.70 ^{+0.09} _{-0.12}	12.72 ^{+0.25} _{-0.03}
SK-67D144	-30, 50	14.07 ^{+0.07} _{-0.06}	-30, 100	14.14 ^{+0.06} _{-0.07}	13.25 ^{+0.21} _{-0.08}
BI184	-30, 50	14.25 ^{+0.04} _{-0.04}	-30, 100	14.48 ^{+0.04} _{-0.04}	13.25 ^{+0.21} _{-0.08}
NGC2004-B15	-30, 50	14.11 ^{+0.10} _{-0.08}	-30, 100	14.22 ^{+0.09} _{-0.12}	9.78 ^{+0.24} _{-0.03}
SK-71D38	-50, 50	14.29 ^{+0.01} _{-0.01}	-50, 100	14.49 ^{+0.04} _{-0.04}	13.39 ^{+0.21} _{-0.08}
SK-71D45	-30, 50	13.81 ^{+0.73} _{-0.34}	-30, 100	14.01 ^{+0.36} _{-0.55}	13.71 ^{+0.41} _{-0.04}
SK-67D166	-20, 50	14.05 ^{+0.04} _{-0.03}	-20, 100	14.28 ^{+0.04} _{-0.04}	12.80 ^{+0.18} _{-0.12}
SK-67D168	-30, 50	13.97 ^{+0.02} _{-0.03}	-30, 100	14.24 ^{+0.02} _{-0.03}	13.04 ^{+0.17} _{-0.13}
SNR0532-675	-70, 50	14.20 ^{+0.04} _{-0.04}	-70, 100	14.38 ^{+0.04} _{-0.05}	13.12 ^{+0.10} _{-0.20}
SK-67D191	-40, 50	14.45 ^{+0.02} _{-0.02}	-40, 100	14.55 ^{+0.01} _{-0.01}	11.28 ^{+0.16} _{-0.14}
HV5936	-30, 50	14.09 ^{+0.05} _{-0.04}	-30, 100	14.34 ^{+0.04} _{-0.04}	13.59 ^{+0.17} _{-0.13}
SK-69D191	-30, 50	14.06 ^{+0.04} _{-0.04}	-30, 100	14.22 ^{+0.04} _{-0.04}	13.90 ^{+0.16} _{-0.14}
J053441-693139	-35, 50	13.94 ^{+0.23} _{-0.15}	-35, 100	14.17 ^{+0.15} _{-0.24}	12.65 ^{+0.30} _{-0.09}
SK-67D211	-40, 50	14.07 ^{+0.06} _{-0.05}	-40, 100	14.12 ^{+0.06} _{-0.06}	11.44 ^{+0.09} _{-0.21}
BREY64	10, 50	13.29 ^{+0.38} _{-0.20}	10, 100	14.21 ^{+0.16} _{-0.25}	13.12 ^{+0.31} _{-0.10}
SNR0536-692	38, 50	13.28 ^{+0.39} _{-0.20}	38, 100	14.06 ^{+0.49} _{-0.23}	13.46 ^{+0.38} _{-0.37}
SK-69D220	-40, 50	14.00 ^{+0.02} _{-0.02}	-40, 100	14.28 ^{+0.02} _{-0.02}	13.44 ^{+0.17} _{-0.13}
SK-66D172	-30, 50	13.87 ^{+0.04} _{-0.04}	-30, 100	14.32 ^{+0.03} _{-0.03}	13.95 ^{+0.18} _{-0.12}
BI253	-20, 50	13.99 ^{+0.05} _{-0.05}	-20, 100	14.34 ^{+0.04} _{-0.04}	13.02 ^{+0.19} _{-0.11}

Table 2 – Continued

Target name	limit (km s ⁻¹)	log N(O VI) (dex)	limit (km s ⁻¹)	log N(O VI) (dex)	log N(O VI) [†] (dex)
SK-68D137	-20, 50	13.50 ^{+0.04} _{-0.04}	-20, 100	14.33 ^{+0.05} _{-0.06}	13.36 ^{+0.20} _{-0.09}
MK42	-20, 50	13.79 ^{+0.12} _{-0.10}	-20, 100	14.40 ^{+0.09} _{-0.11}	13.71 ^{+0.24} _{-0.04}
SK-69D243	10, 50	13.45 ^{+0.14} _{-0.11}	10, 100	14.32 ^{+0.07} _{-0.09}	13.64 ^{+0.23} _{-0.06}
30DOR-S-R136	-30, 50	14.03 ^{+0.13} _{-0.10}	-30, 100	14.16 ^{+0.10} _{-0.16}	10.40 ^{+0.26} _{-0.01}
SK-69D246	-40, 50	14.25 ^{+0.03} _{-0.03}	-40, 100	14.51 ^{+0.03} _{-0.03}	13.57 ^{+0.18} _{-0.12}
HDE269927	-40, 50	14.10 ^{+0.05} _{-0.05}	-40, 100	14.32 ^{+0.05} _{-0.06}	13.12 ^{+0.21} _{-0.09}
SK-69D257	-40, 50	14.21 ^{+0.06} _{-0.05}	-40, 100	14.45 ^{+0.05} _{-0.05}	13.44 ^{+0.20} _{-0.10}
SNR0543-689	0, 50	13.95 ^{+0.06} _{-0.05}	0, 100	14.20 ^{+0.06} _{-0.07}	13.21 ^{+0.22} _{-0.08}
D301-1005	-30, 50	14.16 ^{+0.04} _{-0.04}	-30, 100	14.41 ^{+0.04} _{-0.04}	13.56 ^{+0.19} _{-0.11}
SK-67D250	-40, 50	14.24 ^{+0.04} _{-0.04}	-40, 100	14.29 ^{+0.05} _{-0.04}	11.70 ^{+0.19} _{-0.10}
D301-NW8	-30, 50	13.89 ^{+0.01} _{-0.01}	-30, 100	14.12 ^{+0.07} _{-0.82}	13.06 ^{+0.01} _{-0.20}
SK-70D115	-40, 50	14.26 ^{+0.21} _{-0.14}	-40, 100	14.35 ^{+0.07} _{-0.09}	12.68 ^{+0.23} _{-0.06}

[†] column densities are calculated in the range from 100 km s⁻¹ to the upper limit as given in the column 2 of Table 1 for each sightline.

Table 3. O VI column density [log N(O VI)] value from literature

Region	No. of stars	Mean	Median	Range	Ref.
Galactic Halo	11	14.45	14.47	14.16-14.84	a
Galactic Halo	12	14.52	14.55	14.22-14.67	b
Galactic Halo	22	14.17	14.25	13.65-14.57	c
Local ISM	39	13.05	13.10	12.38-13.60	d
Galactic Disk	148	14.23	—	12.90-14.68	e
Galactic Halo	139	14.11	14.15	13.23-15.03	f

a-(Savage et al. 2000), b-(Howk et al. 2002a), c-(Zsargó, Sembach & Howk 2003), d-(Savage & Lehner 2006), e-(Bowen et al. 2008), f-(Savage & Wakker 2009)

REFERENCES

- Blair W. P., Oliveira C., Lamassa S., et al., 2009, *PASP*, 121, 634
- Bowen D. V., Jenkins B. E., Tripp T. M., et al. 2008, *ApJS*, 176, 59
- Cox D. P., 2005, *ARA&A*, 43, 337
- Bland-Hawthorn, J., et al. 1998, *MNRAS*, 299, 611
- Danforth C. W., Howk J. C., Fullerton A. W., Blair W. P., Sembach K. R., 2002, *ApJS*, 139, 81
- Danforth C. W., Shull J. M., Rosenberg J. L., Stocke J. T., 2006, *ApJ*, 640, 716
- Danforth C. W., Blair W. P., 2006, *ApJ*, 646, 205
- de Boer K.S., Morras, R., & Bajaja, E. 1990, *A&A*, 233, 523
- Dixon W. Van D., Hurwitz M, Ferguson H. C., 1996, *ApJ*, 469, 77
- Dixon W. V. D., Sankrit R., Otte B., 2006, *ApJ*, 647, 328
- Dixon W. V., Sahnou J., Barrett P.E. et al. 2007, *PASP*, 119, 527
- Dixon W. V. D., Sankrit R., 2008, *ApJ*, 686, 1162
- Friedman S. D. et al., 2000, *ApJ*, 538, L39
- Fox A.J., Wakker, B.P., Smoker, J.V., et al. 2010, *ApJ*, 718, 1046
- Fox A.J., Richter, P., Wakker, B.P., et al. 2013, *ApJ*, 772, 110
- Fox A.J., Wakker, B.P., Barger, A., et al. 2014, *ApJ*, 787, 147
- Gardiner L. T. & Noguchi, M. 1996, *MNRAS*, 278, 191
- Heckman T.M., Norman C.A., Strickland D. K. & Sembach K. R., 2002, *ApJ*, 577, 691
- Hoopes C. G., Sembach K. R., Howk J. C., Savage B. D., Fullerton A. W., 2002, *ApJ*, 569, 233
- Howk J. C., Sembach K. R., Savage B. D., Massa D., Friedman S. D., Fullerton A. W., 2002a, *ApJ*, 569, 214
- Howk J. C., Savage B. D., Sembach K. R., Hoopes C. G., 2002b, *ApJ*, 572, 264
- Indebetouw R., Shull J. M., 2004, *ApJ*, 605, 205
- Jenkins E. B., 1978a, *ApJ*, 219, 845
- Jenkins E. B., 1978b, *ApJ*, 220, 107
- Kalberla P.M.W. & Dedes L. 2008, *A&A*, 487, 951
- Lehner N., Howk J. C., 2007, *MNRAS*, 377, 687
- Lehner N., Staveley-Smith L. & Howk J. C. 2009, *ApJ*, 702, 940
- Lehner N., Fullerton A. W., Sembach K. R., Massa D. L., Jenkins E. B., 2001, *ApJ*, 556, L103
- Lehner, N. 2002, *ApJ*, 578, 126
- Lehner N., Fullerton A. W., Massa D., Sembach K. R., Zsargo, J., 2003, *ApJ*, 589, 526
- Lehner N., Howk J. C., 2004, *PASP*, 116, 824
- Lehner N., Zech W. F., Howk J. C. & Savage B. D., 2011, *ApJ*, 727, 46
- Meaburn J., McGee R. X., Newton L. M., 1984, *MNRAS*, 206, 705
- Moos H.W., Cash W.C., Cowie L.L. et al., 2000, *ApJ*, 538, 1
- Oegerle W. R., Jenkins E. B., Shelton R. et al., *ApJ*, 622, 377

- Pathak A., Pradhan A.C., Sujatha N.V. & Murthy J., 2011, MNRAS, 412, 1105
 Putman M.E. et al. 2003, ApJ, 597, 948
 Richter P., de Boer, K.S., Bomans, D.J., et al. 1999, Nature, 402, 386
 Richter P., Fox, A. J., Wakker, B. P., et al. 2013, ApJ, 772, 111

 Sahnou D.J., Moos H.W., Ake T.B. et al., 2000, ApJ, 538, 7
 Sankrit R., Dixon, W. V. D., 2007, PASP, 119, 284
 Savage B. D., Edger, R. & Diplas A. 1990, ApJ, 361, 107
 Sarma, R. et al. 2014, AdSpR, 53, 963
 Savage B. D., Sembach K. R., 1991, ApJ, 379, 245
 Savage B. D. & de Boer K. S., 1981, ApJ, 243, 460

 Savage B. D., Sembach K.R., Jenkins E.B. et al., 2000, ApJ, 538, 27

 Savage B. D. et al., 2003, ApJS, 146, 125

 Savage B. D., Lehner N., 2006, ApJS, 162, 134

 Savage B. D. & Wakker B. P., 2009, ApJ, 702, 1472

 Sembach K. R. & Savage B. D., 1992, ApJS, 83, 147
 Sembach K. R., Savage B. D., Lu L., & Murphy E. M., 1995, ApJ, 451, 616
 Sembach K. R., Savage, B. D., Lu L., & Murphy, E. M., 1999, ApJ, 515, 108
 Shelton R. L. & Cox D. P., 1994, ApJ, 434, 599
 Shelton R. L., Kruk J. W., Murphy E. M., et al., 2001, ApJ, 560, 730
 Spitzer L. J., 1956, ApJ, 124, 20
 Sutherland R.S., & Dopita M.A., 1993, ApJS, 88, 253
 Tepper-Garca T., Richter P., Schaye J., et al. 2011, MNRAS, 413, 190
 Tufte S. L., Reynolds R. J. & Haffner L. M., 1998, ApJ, 504, 773
 Thom C., Putman M. E., Gibson B. K., et al. 2006, ApJ, 638, L97
 Thom C., Peek J. E. G., Putman M. E., et al. 2008, ApJ, 684, 364
 Wakker B. P., Savage B. D., Sembach K. R. et al. 2003, ApJS, 146, 1
 Wakker B. P., York D. G., Howk J. C., et al. 2007, ApJ, 670, L113
 Wakker B. P., York D. G., Wilhelm R., et al. 2008, ApJ, 672, 298
 Wakker B. P., Savage B. D., Fox A. J., Benjamin R. A., Shapiro P. R., 2012, ApJ, 749, 157
 Welsh B. Y., Lallement R., 2008, A&A, 490, 707
 Wannier P., & Wrixon G. T. 1972, ApJL, 173, L119
 Weiner B. J., & Williams T. B. 1996, AJ, 111, 1156
 Welty D. E., Frisch P. C., Sonneborn G., & York D. G. 1999, ApJ, 512, 636
 Yan Z. -C., Tambasco M., Drake G. W. F., 1998, PRA, 57, 1652
 York D.G. 1974, ApJ, 193, 127

 Zsargó J., Sembach K.R. & Howk J.C., 2003, ApJ, 586, 1049